Renormalization-group calculation of excitation properties for impurity models

M. Yoshida
Departamento de Física, Instituto de Geociências e Ciências Exatas, Universidade Estadual Paulista, 13500 Rio Claro, São Paulo, Brazil

M. A. Whitaker and L. N. Oliveira
Departamento de Física e Ciência dos Materiais, Instituto de Física e Química de São Carlos, Universidade de São Paulo, 13560 São Carlos, São Paulo, Brazil

(Received 3 November 1989)

The renormalization-group method developed by Wilson to calculate thermodynamical properties of dilute magnetic alloys is generalized to allow the calculation of dynamical properties of many-body impurity Hamiltonians. As a simple illustration, the impurity spectral density for the resonant-level model (i.e., the $U=0$ Anderson model) is computed. As a second illustration, for the same model, the longitudinal relaxation rate for a nuclear spin coupled to the impurity is calculated as a function of temperature.

I. INTRODUCTION

Strong correlations dominate the physics of dilute magnetic alloys and of fluctuating-valence and heavy-fermion compounds. Analyses of such systems on the basis of single-particle concepts or straightforward perturbative expansions have long been proved unreliable, in many cases even at the qualitative level. Their theory has nevertheless advanced significantly in the past decade, driven by a combination of exact results and controlled approximations. Four techniques—the Bethe ansatz,[1] the renormalization-group[2] and Monte Carlo[3] methods, and the $1/N$ expansion[4]—have played a prominent role in this development. Given that each of them has specific limitations and must be complemented by the other three, attempts to extend the scope of an individual approach are important. This paper is concerned with one such extension.

We consider the renormalization-group method, a technique originally developed to calculate thermodynamical properties of impurity models that more recently has been employed to evaluate dynamical properties of simple (essentially fixed-point) Hamiltonians.[5] Nevertheless, as we shall show, to compute excitation properties *away from fixed points* one has to generalize the renormalization-group transformation in Ref. 2; the necessary generalization is detailed here for the first time. As an illustration of the extended method, we consider an exactly diagonalizable Hamiltonian, that of the $U=0$ spin-degenerate Anderson model[6] and compute two of its dynamical properties: (1) the frequency-dependent impurity spectral density, and (2) the temperature-dependent relaxation rate for a nuclear spin coupled (by a contact interaction) to the impurity spin. Experimental motivation for the first calculation is provided by photoemission and inverse photoemission measurements,[7] and for the second by NMR experiments,[8] but the present work does not discuss experimental data. Our illustrative calculations are aimed at demonstrating that the novel approach solves the technical problem of calculating the excitation properties of impurity many-body Hamiltonians.

The cornerstone of the renormalization-group approach is a logarithmic discretization of the conduction band,[2] which ultimately substitutes a discrete set for the continuum of eigenvalues of the model Hamiltonian. This approximation is justified *a posteriori*: after a physical property for a given model is computed, one must show that the results converge rapidly to the continuum limit. For thermodynamical averages, this task is easily executed.[9,10] For golden-rule calculations, however, a naive application of the discretization in Ref. 2 produces discrete sequences of lines bearing little resemblance to the smooth spectra expected in the continuum limit. In special cases, a rapidly convergent smoothing procedure has been shown to produce accurate results.[5] That procedure nevertheless has two limitations: (1) it applies only to quadratic Hamiltonians or to Hamiltonians that, on the basis of special conservation laws, can be projected onto subspaces in which they become quadratic, and (2) it assumes that the single-particle spectrum of the model Hamiltonian is that of a conduction band with uniform phase shifts. Taken together, these two premises apply only to fixed-point Hamiltonians, in most cases limiting the computation of physical properties to restricted frequency and temperature ranges.

By contrast, the procedure in this paper applies to the entire renormalization-group flow diagram, i.e., to the fixed-point and crossover regions alike. It covers the full parametric space of many-body impurity Hamiltonians and enables us to compute physical properties for all temperatures or frequencies. Our example, the $U=0$ Anderson model, has two fixed points, both thoroughly discussed in Ref. 9: at high (low) energies, the free-orbital (frozen-impurity) fixed point dominates the physical properties of the Hamiltonian. In the renormalization-group approach, therefore, to calculate accurately the intermediate-energy excitation properties of even this

quadratic Hamiltonian one must resort to the generalized procedure we describe.

Our presentation is organized as follows. Section II discusses the Hamiltonians covered by the generalized renormalization-group approach, which is detailed in Sec. III. Sections IV and V are dedicated to the two illustrations. Section VI presents our conclusions and discusses other applications of the new method. Finally, the Appendix collects an algebraic derivation too lengthy to appear in Sec. III.

II. SCOPE OF THE METHOD

This work concerns models comprising a single impurity orbital, denoted c_d, coupled to noninteracting s-wave states c_k centered at the impurity site. The Anderson[6] and the Nozières–De Dominicis[11] Hamiltonians are examples. Assuming the conduction band half filled in momentum space, we measure the momenta k from and in units of the Fermi momentum, so that k ranges from -1 to 1. We also assume that the interaction between conduction band and impurity is short ranged, hence momentum independent, so that the impurity couples to the conduction states through the combination $\int c_k dk$. It is then convenient to define the *normalized* Fermi operator

$$f_0=\frac{1}{\sqrt{2}}\int_{-1}^{1}c_k dk \ . \tag{1}$$

The conduction-band–impurity interaction must be represented by a Hamiltonian involving the operators f_0 and no other combination of the c_k. Thus, in the Anderson model, the impurity and conduction states are coupled by the Hamiltonian[9]

$$H_{i\text{-}c}=\sqrt{2}V(f_0^{\dagger}c_d+c_d^{\dagger}f_0) \ , \tag{2}$$

while the conduction-band and impurity Hamiltonians are

$$H_c=\int_{-1}^{1}\varepsilon_k c_k^{\dagger}c_k dk \ , \tag{3}$$

and

$$H_i=\varepsilon_d c_d^{\dagger}c_d+Un_{d\uparrow}n_{d\downarrow} \ . \tag{4}$$

Following previous applications of the renormalization-group method,[2,5,9,10] we consider a linear dispersion relation ($\varepsilon_k=Dk$, where $2D$ is the bandwidth). The renormalization-group transformation in Sec. III nevertheless applies equally well to nonlinear relations, as a subsequent paper is planned to show.[12]

The analysis in Sec. III is independent of the form of the impurity Hamiltonian. H_i involves only the impurity states c_d and can be easily diagonalized, either numerically or analytically. The direct product of its eigenvectors with the operator f_0 [Eq. (1)] yields a basis that is complete with respect to both the impurity Hamiltonian and the impurity–conduction-band Hamiltonian $H_{i\text{-}c}$. This basis is nonetheless incomplete with respect to the conduction states and must hence be augmented. Before this can be done, however, the renormalization-group approach requires that the conduction band be discretized. Since the discretization in this paper deviates from that in Ref. 2, its discussion deserves a separate section.

III. FORMALISM

A. Discretization of the conduction band

In order to make numerically tractable the model Hamiltonian in Sec. IV, we must discretize the continuum of conduction states. To this end we follow the sequence in Fig. 1, generalizing the logarithmic sequence in Ref. 2. This sequence defines intervals in momentum space. For each of them, out of the infinitely many ways in which its operators c_k can be linearly combined, we consider the combination most localized around the impurity site. In particular, for the interval $1>k>\Lambda^{-z}$, we define the normalized Fermi operator

$$a=(1-\Lambda^{-z})^{-1/2}\int_{\Lambda^{-z}}^{1}c_k dk \ , \tag{5}$$

and for the interval $-1<k<-\Lambda^{-z}$ the operator

$$b=(1-\Lambda^{-z})^{-1/2}\int_{-1}^{-\Lambda^{-z}}c_k dk \ . \tag{6}$$

For each of the intervals $\Lambda^{1-z-m}>k>\Lambda^{-z-m}$ ($m=1,2,\cdots$), we likewise define the operator

$$a_m=\frac{\Lambda^{(m+z-1)/2}}{(1-\Lambda^{-1})^{1/2}}\int_{\Lambda^{-z-m}}^{\Lambda^{1-z-m}}c_k dk \ , \tag{7}$$

and finally, for each of the intervals $-\Lambda^{1-z-m}<k<-\Lambda^{-z-m}$ ($m=1,2,\cdots$) the operator

$$b_m=\frac{\Lambda^{(m+z-1)/2}}{(1-\Lambda^{-1})^{1/2}}\int_{-\Lambda^{1-z-m}}^{-\Lambda^{-z-m}}c_k dk \ . \tag{8}$$

These definitions generalize the original discretization,[2] to which Fig. 1 reduces for $z=1$. We refer the reader to Refs. 2 and 9 for discussions of the approximation involved in projecting the conduction Hamiltonian H_c on the basis $\mathcal{B}$ of the operators a,b,a_m,b_m, a basis clearly incomplete with respect to the operators c_k. Here, we write down the projection obtained[13] by inverting Eqs. (5)–(8) and substituting in Eq. (3) the resulting expressions for c_k:

$$H_c=\sum_{m=1}^{\infty}E_m(z,\Lambda)(a_m^{\dagger}a_m-b_m^{\dagger}b_m)+E_0(z,\Lambda)(a^{\dagger}a-b^{\dagger}b) \ , \tag{9}$$

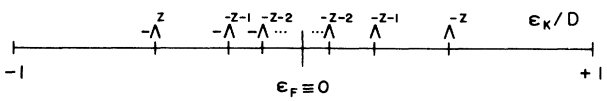

FIG. 1. Logarithmic discretization of the conduction band. The parameter Λ must be larger than unity but is otherwise arbitrary; in numerical calculations, a typical choice is $\Lambda=3$. The parameter z lies in the interval $0<z\leq 1$. For $z=1$, we recover the discretization in Refs. 2 and 9. In this case, for a linear dispersion relation, the codiagonal coefficients ε_n on the right-hand side of Eq. (13) have been determined analytically (see Ref. 2).

where

$$E_m(z,\Lambda)=\int_{\Lambda^{-z-m}}^{\Lambda^{1-z-m}}\varepsilon_k dk \Big/ \int_{\Lambda^{-z-m}}^{\Lambda^{1-z-m}} dk \ , \tag{10}$$

and

$$E_0(z,\Lambda)=\int_{\Lambda^{-z}}^{1}\varepsilon_k dk \Big/ \int_{\Lambda^{-z}}^{1} dk \ . \tag{11}$$

Each energy $\pm E_m(z,\Lambda)$ or $\pm E_0(z,\Lambda)$, appearing on the right-hand side of Eq. (9), is the average kinetic energy in the corresponding intervals depicted in Fig. 1. For given Λ and fixed z, these energies form a discrete set, so that, as the example in Sec. IV will show, the golden-rule calculation of photoemission rates for the discretized Hamiltonian yields discrete transition lines instead of the continuous absorption spectra one would expect. When z runs from 0 to 1, however, the energies $\pm E_m(z,\Lambda)$ and $\pm E_0(z,\Lambda)$ cover the entire conduction band, turning the golden-rule transition lines into a continuous spectrum. This smoothing procedure, detailed in Sec. IV, provides the motivation for introducing the parameter z in Fig. 1.

The operator f_0, Eq. (1), can also be projected on the basis $\mathcal{B}$. By inverting Eqs. (5)–(8) we find

$$f_0=\left[\frac{1-\Lambda^{-1}}{2}\right]^{1/2}\sum_{m=1}^{\infty}\Lambda^{(1-z-m)/2}(a_m+b_m) + \left[\frac{1-\Lambda^{-z}}{2}\right]^{1/2}(a+b) \ . \tag{12}$$

Unlike Eq. (9), this equality is exact; this can be checked by substituting the right-hand sides of Eqs. (5)–(8) for the operators a, b, a_m, and b_m, respectively. Exact, therefore, is the projection of the interaction $H_{i\text{-}c}$ [e.g., Eq. (2)] on the discrete basis $\mathcal{B}$. Only the conduction Hamiltonian is affected by the discretization in Fig. 1. This circumstance results from the definition of the operators a, b, a_m, and b_m, the first of two precautions[2] taken to make the accuracy of the numerical calculations model parameter independent. The second precaution[2] involves the tridiagonalization of the conduction Hamiltonian, to which we now turn.

B. Tridiagonalization of the conduction Hamiltonian

The infinite basis $\mathcal{B}$ must be made finite before the model Hamiltonian can be diagonalized numerically. At first sight, one would be tempted to truncate at finite m the infinite sum on the right-hand side of Eq. (9). This must nevertheless be avoided. For then a parallel truncation on the right-hand side of Eq. (12) would be necessary, affecting the coupling between impurity and conduction electrons and making the accuracy of all subsequent computations dependent on the strength of $H_{i\text{-}c}$.

We therefore introduce a new basis. We construct an orthonormal, infinite sequence of Fermi operators f_n ($n=0,1,2,\cdots$), where f_0 is the operator in Eq. (12), and the other operators are defined by the Lanczos[14] construction, i.e., by requiring the conduction Hamiltonian to have the tridiagonal form

$$H_c=\sum_{n=0}^{\infty}\varepsilon_n^z(f_n^{\dagger}f_{n+1}+\text{H.c.}) \ . \tag{13}$$

As the Appendix shows, this condition leads to an equation determining the coefficients ε_n^z:

$$\prod_{n=0}^{N}(\varepsilon_n^z)^2=F_N(z,\Lambda)-[(\mathcal{H}_{N+1})^{2N+2}]_{11} \ , \tag{14}$$

where the term within the square brackets on the right-hand side is the $2N+2$th power of the matrix

$$[\mathcal{H}_{N+1}]_{ij}=\varepsilon_{i-1}^z\delta_{i,j-1}+\varepsilon_{j-1}^z\delta_{j,i-1} \ , \quad (i,j=1,2,\cdots,N+1) \ , \tag{15}$$

and

$$F_N(z,\Lambda)=(1-\Lambda^{-1})\sum_{m=1}^{\infty}\Lambda^{1-z-m}[E_m(z,\Lambda)]^{2N+2} + (1-\Lambda^{-z})[E_0(z,\Lambda)]^{2N+2} \ . \tag{16}$$

Equation (14) is solved iteratively. For $N=0$, it determines ε_0^z:

$$(\varepsilon_0^z)^2=(1-\Lambda^{-1})\sum_{m=1}^{\infty}\Lambda^{1-z-m}[E_m(z,\Lambda)]^2 + (1-\Lambda^{-z})[E_0(z,\Lambda)]^2 \ . \tag{17}$$

For $N>0$, Eq. (16) determines $F_N(z,\Lambda)$, and provided that $\varepsilon_0^z,\varepsilon_1^z,\cdots,\varepsilon_{N-1}^z$ have been determined, the matrix $(\mathcal{H}_{N+1})^{2N+2}$ can be computed from Eq. (15). Equation (14) then determines ε_N^z.

For small N ($N\le\hat{N}$, where $\hat{N}$ depends on Λ and on the dispersion relation—a typical value is 5), this straightforward procedure can be carried out analytically or numerically.[15] For larger N, however, a practical difficulty arises, deserving a brief digression. For increasing n, the coefficients ε_n^z decrease rapidly; for a linear dispersion relation and $z=1$, for example, one finds[2]

$$\varepsilon_n^z=D(1+\Lambda^{-1})\Lambda^{-n/2}/2 \quad (n\gg 1,\ \varepsilon_k=Dk, \text{ and } z=1) \ . \tag{18}$$

As N decreases, therefore, both sides of Eq. (14) become small. Since neither of the two terms on the right-hand side diminishes appreciably, the small ε_N^z must be computed from the difference between two relatively large numbers and for $N>\hat{N}$ the procedure grows inaccurate.

In practice, this problem is minor. Quadrupule-precision numerical computations make $\hat{N}\ge 10$, and symbolic-manipulation programs make $\hat{N}$ arbitrarily large. On the other hand, as shown following, for $N\to\infty$ an asymptotic expression for the ε_N^z can be easily derived. As it turns out, this expression, denoted $\hat{\varepsilon}_N^z$, describes accurately (to four significant digits, typically) the ε_N^z even for N as small as 10. Thus, for $N\le\hat{N}\approx 10$ Eqs. (14) and (15) determine ε_N^z, while for $N>\hat{N}$ the asymptotic form $\hat{\varepsilon}_N^z$ is substituted for ε_N^z. The difference between ε_N^z and $\hat{\varepsilon}_N^z$ (an upper bound for the error in this approximation) is insignificant. An illustration will be presented in Sec. IV B.

In order to find the asymptotic coefficients $\hat{\varepsilon}_N^z$, we consider the conduction energies near the Fermi level. For

these, the dispersion relation can be linearized, yielding $\varepsilon_k \simeq v_F k$ ($k \ll 1$), where v_F is the Fermi velocity. Substitution in the numerator on the right-hand side of Eq. (10) then leads to

$$E_m(z,\Lambda) \cong \left[\frac{v_F \Lambda^{1-z}}{D}\right] \frac{D(1+\Lambda^{-1})\Lambda^{-m}}{2} \quad (m \gg 1) . \tag{19}$$

The right-hand side of this equation has been factored so that the term within large parentheses on the right-hand side, a constant for fixed Λ and z, multiplies the discrete energies $D(1+\Lambda^{-1})\Lambda^{-m}/2$, precisely the energies that result[2] when a linear dispersion relation is discretized for $z=1$. Since the coefficients ε_N^z scale linearly with any constant factor multiplying the conduction energies ε_k, and hence with any factor multiplying the energies $E_m(z,\Lambda)$, the asymptotic form for ε_N^z is obtained by multiplying the right-hand side of Eq. (18) by the term within large parentheses in Eq. (19):

$$\hat{\varepsilon}_n^z = \frac{1+\Lambda^{-1}}{2} v_F \Lambda^{1-z-n/2} . \tag{20}$$

C. Truncation of the conduction Hamiltonian

With Eq. (20) and Eqs. (14)–(16), a conduction Hamiltonian with arbitrary dispersion relation can be made tridiagonal. Since $\varepsilon_n^z \to 0$ for $n \to \infty$, for given energy ε one can always find an integer N such that

$$\varepsilon_N^z \ll \varepsilon . \tag{21}$$

Thus, if one is interested in calculating excitation properties at the energy ε (or at the temperature $T=\varepsilon/k_B$, where k_B is Boltzmann's constant), negligible error will result from truncating at $n=N$ the infinite series on the right-hand side of Eq. (13); moreover, since the conduction-band–impurity Hamiltonian $H_{i\text{-}c}$ commutes with the operators f_n ($n>0$), this error is independent of the impurity–conduction-band interaction.

With the truncated form substituted for the conduction-band Hamiltonian, the model Hamiltonian H becomes

$$H_{\text{trunc}} = H_i + H_{c\text{-}i} + \sum_{n=0}^{N-1} \varepsilon_n^z (f_n^\dagger f_{n+1} + \text{H.c.}) . \tag{22}$$

On the right-hand side of this expression, the smallest coefficient is

$$\varepsilon_{N-1}^z \approx \hat{\varepsilon}_{N-1}^z = (1+\Lambda^{-1})\Lambda^{-(N-1)/2+1-z} v_F/2$$

[see Eq. (20)]. Following Ref. 2, to define a dimensionless Hamiltonian H_N whose smallest coefficient is ≈ 1, we scale H_{trunc} by $1/\hat{\varepsilon}_{N-1}^z$, defining

$$H_N = \frac{2}{1+\Lambda^{-1}} \Lambda^{(N-1)/2+z-1} \frac{H_{\text{trunc}}}{v_F} . \tag{23}$$

In the large-N limit, this equality in turn defines a renormalization-group transformation $\mathcal{T}$:

$$\mathcal{T}[H_N] \equiv \sqrt{\Lambda} H_N + (f_N^\dagger f_{N+1} + \text{H.c.}) \approx H_{N+1} . \tag{24}$$

While this transformation, essentially identical to the one discussed by Wilson, has no interesting fixed points,[2] the conduction Hamiltonian is an important fixed point of the transformation $\mathcal{R} \equiv \mathcal{T}^2$. In order to show this, that our analysis preserves the scaling[2] of the conduction band, the following section discusses the specific case of a linear dispersion relation.

D. Linear dispersion relation

In order to apply the tridiagonalization procedure in Secs. III A and III B to the linear dispersion $\varepsilon_k = kD$, we must first determine the discrete energies $E_0(z,\Lambda)$ and $E_m(z,\Lambda)$ ($m=1,2,\ldots$). Equations (10) and (11) yield

$$E_m(z,\Lambda) = D \frac{1+\Lambda^{-1}}{2} \Lambda^{1-z-m} , \tag{25}$$

and

$$E_0(z,\Lambda) = D \frac{1+\Lambda^{-z}}{2} , \tag{26}$$

respectively.

TABLE I. Codiagonal coefficients for linear dispersion relation calculated for $\Lambda=3$ and $z=1$ from the numerical procedure defined by Eq. (14) (ε_n^z), from the exact expression in Ref. 2 [ε_n(exact)], and from the asymptotic expression (20).

n	ε_n^z/D	ε_n(exact)$/D$	$\hat{\varepsilon}_n^z/D$
0	$5.547\,001\,96\times10^{-1}$	$5.547\,001\,96\times10^{-1}$	$6.666\,666\,67\times10^{-1}$
1	$3.493\,705\,17\times10^{-1}$	$3.493\,705\,17\times10^{-1}$	$3.849\,001\,79\times10^{-1}$
2	$2.144\,824\,87\times10^{-1}$	$2.144\,824\,87\times10^{-1}$	$2.222\,222\,22\times10^{-1}$
3	$1.267\,483\,08\times10^{-1}$	$1.267\,483\,08\times10^{-1}$	$1.283\,000\,60\times10^{-1}$
4	$7.377\,132\,47\times10^{-2}$	$7.377\,132\,47\times10^{-2}$	$7.407\,407\,41\times10^{-2}$
5	$4.270\,815\,57\times10^{-2}$	$4.270\,815\,57\times10^{-2}$	$4.276\,668\,66\times10^{-2}$
6	$2.468\,007\,66\times10^{-2}$	$2.468\,007\,66\times10^{-2}$	$2.469\,135\,80\times10^{-2}$
7	$1.425\,339\,00\times10^{-2}$	$1.425\,339\,00\times10^{-2}$	$1.425\,556\,22\times10^{-2}$
8	$8.230\,034\,56\times10^{-3}$	$8.230\,034\,56\times10^{-3}$	$8.230\,452\,67\times10^{-3}$
9	$4.751\,773\,60\times10^{-3}$	$4.751\,773\,60\times10^{-3}$	$4.751\,854\,07\times10^{-3}$
10	$2.743\,468\,78\times10^{-3}$	$2.743\,468\,74\times10^{-3}$	$2.743\,484\,22\times10^{-3}$
11	$1.587\,940\,10\times10^{-3}$	$1.583\,948\,37\times10^{-3}$	$1.583\,951\,35\times10^{-3}$

TABLE II. Codiagonal coefficients for linear dispersion relation calculated for $\Lambda=3$ and $z=0.5$ from the numerical procedure defined by Eq. (14) (ε_n^z), and from the asymptotic expression (20). The exact expression in Ref. 2 applies only to $z=1$.

n	ε_n^z/D	$\hat{\varepsilon}_n^z/D$
0	$5.675\,448\,21\times10^{-1}$	$1.154\,700\,54$
1	$4.603\,125\,52\times10^{-1}$	$6.666\,666\,67\times10^{-1}$
2	$4.035\,445\,80\times10^{-1}$	$3.849\,001\,79\times10^{-1}$
3	$2.551\,833\,71\times10^{-1}$	$2.222\,222\,22\times10^{-1}$
4	$1.353\,390\,32\times10^{-1}$	$1.283\,000\,60\times10^{-1}$
5	$7.508\,181\,75\times10^{-2}$	$7.407\,407\,41\times10^{-2}$
6	$4.293\,512\,36\times10^{-2}$	$4.276\,668\,66\times10^{-2}$
7	$2.472\,254\,88\times10^{-2}$	$2.469\,135\,80\times10^{-2}$
8	$1.426\,149\,66\times10^{-2}$	$1.425\,556\,22\times10^{-2}$
9	$8.231\,590\,55\times10^{-3}$	$8.230\,452\,67\times10^{-3}$
10	$4.752\,072\,78\times10^{-3}$	$4.751\,854\,07\times10^{-3}$
11	$2.743\,526\,76\times10^{-3}$	$2.743\,484\,22\times10^{-3}$

Next, we must determine the function $F_N(z,\Lambda)$ appearing on the right-hand side of Eq. (14). From Eq. (16) we find

$$F_N(z,\Lambda)=(1-\Lambda^{-z})\left[\frac{1+\Lambda^{-z}}{2}\right]^{2N+2}+(1-\Lambda^{-1})\left[\frac{1+\Lambda^{-1}}{2}\right]^{2N+2}\frac{\Lambda^{-(2N+3)z}}{1-\Lambda^{-(2N+3)}}\ . \tag{27}$$

Equation (14) is now solved numerically, as explained in Sec. III B. Tables I and II show codiagonal coefficients ε_n^z computed in quadrupole precision for two z's (1 and 0.5, respectively). For comparison, they also list the asymptotic values produced by Eq. (20), indicating that for $n=10$ the numerical and asymptotic ε_n^z agree to four significant digits. For $n\le10$, on the other hand, the numerical procedure in Sec. III B yields coefficients ε_n^z correct to eight significant digits; this is shown by Table I ($z=1$), which compares them to the coefficients ε_n given by the exact expression in Ref. 2. The same comparison shows that, as explained in Sec. III B, the numerical procedure determining the coefficients deteriorates rapidly for $n\ge\hat{N}=11$. Thus, by substituting the asymptotic forms $\hat{\varepsilon}_n^z$ for the ε_n^z ($n\ge11$), we ensure that the codiagonal coefficients of the conduction Hamiltonian deviate less than 0.1% from the exact coefficients.

TABLE IV. Positive eigenvalues $\hat{\eta}_j$ ($j=1,\cdots,N/2$) of the truncated conduction Hamiltonian H_N [Eq. (28)] for two even N's (16 and 18) and two z's (1 and 0.5).

	$z=1$		$z=0.5$	
Eigenvalue	$N=16$	$N=18$	$N=16$	$N=18$
η_1	1.695 755	1.695 755	1.695 747	1.695 752
η_2	5.196 104	5.196 099	5.196 034	5.196 075
η_3	15.588 52	15.588 48	15.587 97	15.588 27
η_4	46.765 38	46.765 55	46.765 27	46.763 90
η_5	140.296	140.296 2	140.296 1	140.295 8
η_6	420.888	420.888 4	420.888 3	420.888 3
η_7	1 262.66	1 262.665	1 262.665	1 262.665
η_8	3 787.99	3 787.995	2 587.249	3 787.995
η_9		11 363.99		7 761.746

Having obtained the codiagonal coefficients ε_n, we can now write and diagonalize the truncated Hamiltonian H_N. As an illustration, we consider the conduction-band Hamiltonian, i.e., we choose $H_i=H_{i\text{-}c}=0$. Equation (23) in this case becomes

$$H_N=\Lambda^{(N-1)/2}\sum_{n=0}^{N-1}\xi_n^z(f_n^\dagger f_{n+1}+\text{H.c.})\ , \tag{28}$$

where

$$\xi_n^z=\frac{2}{1+\Lambda^{-1}}\frac{\varepsilon_n^z}{D}\Lambda^{z-1}\ . \tag{29}$$

To diagonalize H_N, we write Eq. (28) in the following form:

$$H_N=\sum_{m,n=0}^{N}f_m^\dagger\mathcal{H}_{m,n}f_n\ , \tag{30}$$

TABLE III. Positive eigenvalues η_j [$j=1,\cdots,(N+1)/2$] of the truncated conduction Hamiltonian H_N [Eq. (28)] for three odd N's (15, 17, and 25) and two z's (1 and 0.5).

	$z=1$			$z=0.5$		
Eigenvalue	$N=15$	$N=17$	$N=25$	$N=15$	$N=17$	$N=25$
η_1	0.800 048 3	0.800 047 9	0.800 047 7	0.800 042 9	0.800 046 1	0.800 047 7
η_2	2.997 492	2.997 489	2.997 487	2.997 451	2.997 475	2.997 487
η_3	9.000 034	9.000 013	9.000 000	8.999 716	8.999 891	8.999 998
η_4	27.000 01	27.000 10	27.000 00	26.999 94	26.999 15	26.999 99
η_5	81.000 00	81.000 02	81.000 01	81.000 00	80.999 83	80.999 89
η_6	243.000 0	243.000 0	243.000 1	243.000 0	243.000 0	242.999 0
η_7	729.000 0	729.000 0	729.001 1	729.000 0	729.000 0	728.991 2
η_8	2 187.000	2 187.000	2 187.008	1 493.749	2 187.000	2 186.931
η_9		6 561.000	6 561.002		4 481.246	6 560.986
η_{10}			19 683.00			19 683.00
η_{11}			59 049.00			59 049.00
η_{12}			177 147.0			177 147.0
η_{13}			531 441.0			362 981.0

with

$$\mathcal{H}_{m,n}=\Lambda^{(N-1)/2}(\xi_n\delta_{m,n+1}+\xi_m\delta_{n,m+1}) \quad (m,n=0,\ldots,N)\ . \tag{31}$$

The Hermitian matrix $\mathcal{H}$ can be diagonalized numerically. The results for $z=1$ and 0.5, and for various N are displayed in Tables III and IV. For large, odd N, the $N+1$ eigenvalues form a symmetrical set. Each positive (negative) eigenvalue is approximately given by η_j $(-\eta_j)$ $[j=1,\ldots,(N+1)/2]$, where, as Table III shows,

$$\eta_j=\Lambda^{j-1} \quad [j=1,\ldots,(N-1)/2]\ , \tag{32}$$

and

$$\eta_{(N+1)/2}=\frac{1+\Lambda^{-z}}{1+\Lambda^{-1}}\Lambda^{(N-1)/2+z-1}\ . \tag{33}$$

Likewise, for large, even N, the $N+1$ eigenvalues form a symmetrical set, one of them always being zero. Of the remaining ones, each positive (negative) eigenvalue is approximately given by $\hat{\eta}_j$ $(-\hat{\eta}_j)$, where, as Table IV shows,

$$\hat{\eta}_j=\Lambda^{j-1/2} \quad [j=1,\cdots,(N-2)/2]\ , \tag{34}$$

and

$$\hat{\eta}_{N/2}=\frac{1+\Lambda^{-z}}{1+\Lambda^{-1}}\Lambda^{(N-1)/2+z-1}\ . \tag{35}$$

As discussed in Refs. 2 and 9, the eigenvalue $\hat{\eta}_0=0$ results from the particle-hole symmetry of the conduction Hamiltonian (i.e., its invariance under the transformation $c_k\rightarrow c_k^\dagger$). Preserved by the approximations in Secs. III A–III D, this invariance makes the spectrum of H_c symmetrical. For even N, the truncated Hamiltonian has an odd number $(N+1)$ of eigenvalues, so that one of them must vanish.

The results in Tables III and IV, which show that for large N the scaled conduction-band Hamiltonian in Eq. (28) approaches a fixed point of the renormalization-group transformation $\mathcal{R}$, have a simple interpretation.[2,9] In order to obtain the eigenvalues $\pm\mathcal{E}_j$ of the conduction Hamiltonian H_c from those of H_N, we have to multiply the latter by $(1+\Lambda^{-1})\Lambda^{-(N-1)/2+1-z}v_F/2$. For odd N, for instance, we find

$$\mathcal{E}_j=\frac{1+\Lambda^{-1}}{2}\Lambda^{-(N-1)/2+1-z}D\eta_j \quad [j=1,\ldots,(N+1)/2]\ , \tag{36}$$

or with the index $m=(N+1)/2-j$ and Eqs. (34) and (35) substituted for η_j,

$$E_m\equiv\mathcal{E}_j\approx\frac{1+\Lambda^{-1}}{2}D\Lambda^{1-z-m} \quad [m=1,\ldots,(N-1)/2] \tag{37}$$

and

$$E_0\approx\frac{1+\Lambda^{-z}}{2}D\ . \tag{38}$$

The expressions on the right-hand sides of Eqs. (37) and (38) coincide with those on the right-hand sides of Eqs. (25) and (26), respectively. For odd (even) N, the eigenvalues of the truncated Hamiltonian thus reproduce very well the $N+1$ (N) highest energy levels of the discretized conduction Hamiltonian. As one might expect, the central effect of the approximation in Sec. III C is to truncate the infinite series on the right-hand side of Eq. (9).

This simple illustration shows that the more general discretization in Fig. 1 preserves the essential properties of the renormalization-group approach in Ref. 2. The parameter z makes that approach more flexible, as the calculation of excitation properties in Secs. IV and V will show.

IV. IMPURITY SPECTRAL DENSITY FOR THE RESONANT-LEVEL MODEL

A. Computation of the spectral density

This section computes the impurity spectral density for the resonant-level model, a spinless Hamiltonian equivalent to the $U=0$ Anderson Hamiltonian [Eqs. (2)–(4)]. The resonant-level model has three characteristic energies: the band half width D, the impurity-orbital energy ε_d, and the half width[6] $\Gamma=\pi V^2/D$ of the resonance introduced in the conduction band by the coupling to the impurity states. If the latter two were zero, at low energies (i.e., for energies ε much smaller than the width D) the energy-scaling invariance of the conduction band would make the Hamiltonian H approach the fixed point discussed in Sec. III D. The two characteristic energies ε_d and Γ break the scaling invariance and, as shown following, drive the Hamiltonian away from that fixed point.

To demonstrate this and to calculate the impurity spectral density, we first observe that for the resonant-level Hamiltonian, Eq. (23) becomes

$$H_N=\Lambda^{(N-1)/2}\left[\varepsilon_d^z c_d^\dagger c_d+V^z(f_0^\dagger c_d+\text{H.c.})+\sum_{n=0}^{N-1}(\xi_n^z f_n^\dagger f_{n+1}+\text{H.c.})\right]\ , \tag{39}$$

where

$$\varepsilon_d^z=\frac{\varepsilon_d}{D}\frac{2}{1+\Lambda^{-1}}\Lambda^{z-1}\ , \tag{40}$$

and

$$V^z=\frac{V}{D}\frac{2\sqrt{2}}{1+\Lambda^{-1}}\Lambda^{z-1}\ . \tag{41}$$

This quadratic Hamiltonian is easily diagonalized.[9] For odd N, the following results are relevant to our analysis.

(i) *Half of the $N+1$ eigenvalues of H_N are positive, and half are negative, denoted η_{j+} and $-\eta_{j-}$, respectively, where $j=1,\ldots,(N+1)/2$. To an excellent approximation, the following expression determines these eigenvalues:*

$$\eta_{j\pm}\approx\Lambda^{j-1-\gamma_{j\pm}} , \tag{42}$$

where

$$\tan(\pi\gamma_{j\pm})=\frac{\overline{\Gamma}}{(\varepsilon_d-E_{j\pm})} , \tag{43}$$

with

$$E_{j\pm}=\pm\frac{1+\Lambda^{-1}}{2}D\Lambda^{-(N-1)/2+1-z}\eta_{j\pm} , \tag{44}$$

$$\overline{\Gamma}=\frac{\Gamma}{A_\Lambda} , \tag{45}$$

and

$$A_\Lambda=\frac{1+\Lambda^{-1}}{1-\Lambda^{-1}}\frac{\ln\Lambda}{2} . \tag{46}$$

(ii) *The Hamiltonian is diagonalized by the Fermi operators*

$$a_{j\pm}=u_{j\pm}c_d+\sum_{n=0}^{N-1}u_{jn\pm}f_n . \tag{47}$$

In particular, the coefficient of the impurity operator c_d is

$$u_{j\pm}\approx\frac{\sin(\pi\gamma_{j\pm})}{(\sin^2(\pi\gamma_{j\pm})\pm\pi\overline{\Gamma}/(E_{j\pm}\ln\Lambda))^{1/2}} . \tag{48}$$

With these results, we are in a position to calculate the impurity spectral density, defined for fixed z as

$$\rho_d^z(\varepsilon)=\begin{cases}\sum_F|\langle F|c_d^\dagger|\Omega\rangle|^2\delta(E_F-E_\Omega-\varepsilon) & \text{if } \varepsilon>0\\ \sum_F|\langle F|c_d|\Omega\rangle|^2\delta(E_F-E_\Omega-\varepsilon) & \text{if } \varepsilon<0 ,\end{cases} \tag{49}$$

where $|\Omega\rangle$ and $|F\rangle$, energies E_Ω and E_F, are the ground state and an eigenstate of H_N, respectively. For the resonant-level Hamiltonian, the right-hand side of Eq. (49) will vanish unless, for some j $[1\le j\le(N+1)/2]$,

$$|F\rangle=\begin{cases}a_{j+}^\dagger|\Omega\rangle & \text{if } \varepsilon>0\\ a_{j-}|\Omega\rangle & \text{if } \varepsilon<0\end{cases} \tag{50}$$

so that, for $\varepsilon>0$,

$$\langle F|c_d^\dagger|\Omega\rangle=\{c_d^\dagger,a_{j+}\}=u_{j+} , \tag{51}$$

while for $\varepsilon<0$,

$$\langle F|c_d|\Omega\rangle=\{c_d,a_{j-}^\dagger\}=u_{j-} . \tag{52}$$

In general, therefore,

$$\rho_d^z(\varepsilon)=\sum_j u_{j\pm}^2\delta(\varepsilon-E_{j\pm}) , \tag{53}$$

the upper (lower) sign applying for positive (negative) ε.

The right-hand side of this equation, comprising a sequence of δ functions, must be smoothed to produce a continuous spectral density. To this end, we integrate ρ_d^z over the discretization parameter z:

$$\rho_d(\varepsilon)=\int_0^1\rho_d^z(\varepsilon)dz=\int_0^1\sum_j u_{j\pm}^2\delta(\varepsilon-E_{j\pm})dz . \tag{54}$$

It follows that

$$\rho_d(\varepsilon)=\left.\frac{u_{j\pm}^2}{|dE_{j\pm}/dz|}\right|_{E_{j\pm}=\varepsilon} , \tag{55}$$

or substituting Eq. (48) for $u_{j\pm}$,

$$\rho_d(\varepsilon)=\left.\frac{\sin^2(\pi\gamma_{j\pm})}{(\sin^2(\pi\gamma_{j\pm})\pm\pi\overline{\Gamma}/(E_{j\pm}\ln\Lambda))|dE_{j\pm}/dz|}\right|_{E_{j\pm}=\varepsilon} . \tag{56}$$

The derivative in the denominator on the right-hand side is easily computed from Eqs. (42) and (43), which yield

$$\left|\frac{dE_{j\pm}}{dz}\right|=\frac{\pi\overline{\Gamma}}{\sin^2(\pi\gamma_{j\pm})\pm\pi\overline{\Gamma}/(E_{j\pm}\ln\Lambda)} . \tag{57}$$

Equation (56) then becomes

$$\rho_d(\varepsilon)=\left.\frac{\sin^2(\pi\gamma_{j\pm})}{\pi\overline{\Gamma}}\right|_{E_{j\pm}=\varepsilon} . \tag{58}$$

Simple trigonometric identities applied to Eq. (43) then turn Eq. (58) into

$$\rho_d(\varepsilon)=\frac{1}{\pi}\frac{\overline{\Gamma}}{\overline{\Gamma}^2+(\varepsilon_d-\varepsilon)^2} . \tag{59}$$

For $\Lambda\to1$, A_Λ [Eq. (46)] converges rapidly to unity, $\overline{\Gamma}$ [Eq. (45)] converges rapidly to Γ, and Eq. (59) reduces to the exact expression[16]

$$\rho_d(\varepsilon)=\frac{1}{\pi}\frac{\Gamma}{\Gamma^2+(\varepsilon_d-\varepsilon)^2} . \tag{60}$$

For $\Lambda>1$, the substitution $V\to V\sqrt{A_\Lambda}$, a standard procedure in renormalization-group calculations,[17] reduces Eq. (59) to Eq. (60).

It should be noticed that this derivation, although producing the exact expression for the spectral density, involves the errors in Eqs. (42) and (48). A numerical calculation based on the procedure in Sec. III would hence produce results in slight disagreement with Eq. (60). For $j\ge2$, the relative errors in Eqs. (42) and (48) are nevertheless $<1\%$; moreover, these errors diminish rapidly as j increases. The renormalization-group derivation is therefore essentially exact.

B. Comparison with previous renormalization-group computations

Having derived Eq. (60), we now pause to compare the procedure in Ref. 5 with the one in Sec. III. The former approach, which amounts to convoluting the golden rule with a smoothing function, yields the following expression for the impurity spectral density:

$$\rho_d(\varepsilon)=\begin{cases}\sum_F{}'\dfrac{|\langle F|c_d^\dagger|\Omega\rangle|^2}{(E_F-E_\Omega)\ln\Lambda} & \text{for } \varepsilon>0\\ \sum_F{}'\dfrac{|\langle F|c_d|\Omega\rangle|^2}{(E_\Omega-E_F)\ln\Lambda} & \text{for } \varepsilon<0 ,\end{cases} \tag{61}$$

where the prime restricts the sum to eigenstates F of H such that

$$\frac{1}{\sqrt{\Lambda}} \leq \left| \frac{E_F - E_\Omega}{\varepsilon} \right| \leq \sqrt{\Lambda} \ . \tag{62}$$

An analysis similar to that transforming Eq. (49) into Eq. (56) converts Eq. (61) into

$$\rho_d(\varepsilon) = \left. \frac{\sin^2(\pi\gamma_{j\pm})}{(\sin^2(\pi\gamma_{j\pm}) \pm \pi\bar{\Gamma}/(E_{j\pm}\ln\Lambda))|E_{j\pm}|\ln\Lambda} \right|_{E_{j\pm}=\varepsilon} . \tag{63}$$

Compare now the right-hand sides of this expression and Eq. (56). Since their numerators are identical, the two fractions will be equal if and only if

$$\left| \frac{dE_{j\pm}}{dz} \right| = |E_{j\pm}|\ln\Lambda \ . \tag{64}$$

From Eqs. (42) and (44) it then follows that $\gamma_{j\pm}$ must be independent of z. As the following reasoning shows, this condition will only be satisfied if H_N is a fixed point of the transformation $\mathcal{R}$, defined in Sec. III D.

The eigenvalues of a fixed point H_N^* of the transformation $\mathcal{R}$ remain invariant as $N \to N+2$. For the Hamiltonian H_N to be such a fixed point it is therefore necessary that its eigenvalues $\eta_{j\pm}$—hence that the $\gamma_{j\pm}$ [cf. Eq. (43)]—remain invariant as $N \to N+2$, i.e., as $E_{j\pm} \to \Lambda E_{j\pm}$ [see Eq. (44)]. According to Eq. (43), this is possible under two circumstances: (i) $\Gamma = 0$ and $\varepsilon_d = 0$, or (ii) $\Gamma \to \infty$ and $|\varepsilon_d| \to \infty$ (or $\varepsilon_d = 0$). In case (i), $\gamma_{j\pm} = 0$, and we recover the *(free-orbital[9])* fixed point discussed in Sec. III. In case (ii), $\pi\gamma_{j\pm} = \arctan(\bar{\Gamma}/\varepsilon_d)$, and we recover the *(frozen-impurity[10])* fixed point.

In general, one is interested in finite parameters Γ and ε_d, so that H_N is no fixed point of $\mathcal{R}$. Nevertheless, for energies ε such that $|\varepsilon| \gg \Gamma, |\varepsilon_d|$, the Hamiltonian H_N [where Eq. (21) defines N] is close to the free-orbital fixed point. Likewise, for $|\varepsilon| \ll \Gamma, |\varepsilon_d|$, the Hamiltonian H_N is close to the frozen-impurity fixed point. In these two ranges of energies, therefore, the properties of the model Hamiltonian are approximately described by the fixed-point Hamiltonians, the $\gamma_{j\pm}$ are approximately independent of z, and Eq. (64) is a good approximation for the derivative in the denominator of Eq. (56). In these two ranges, therefore, Eq. (63)—i.e., the procedure in Ref. 5—can be justified.

By contrast, for $\varepsilon \approx \min(\Gamma, |\varepsilon_d|)$, as Eq. (43) indicates, the $\gamma_{j\pm}$ depend strongly on $E_{j\pm}$, hence on z, so that Eq. (64) is a poor approximation, and Eq. (56) badly underestimates the spectral density $\rho_d(\varepsilon)$. In this case, the generalized discretization in Fig. 1 is indispensable.

As an illustration, Fig. 2 shows the spectral densities computed from Eqs. (60) and (63) and two impurity energies, 0 and $0.05D$. For both ε_d, for $|\varepsilon| < \Gamma = 0.01D$ the Hamiltonian H_N [Eq. (39)] approaches the frozen-impurity fixed point, a region to which the procedure in Ref. 5 applies. Thus, in both cases, in the limit $\varepsilon \to 0$ the solid circles representing Eq. (63) agree well with the

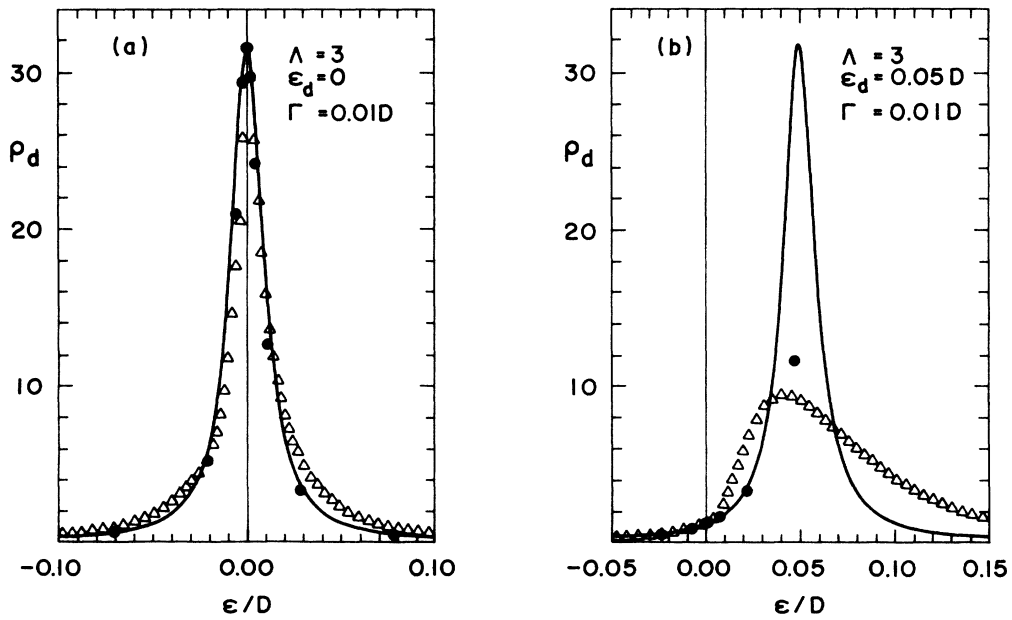

FIG. 2. d-level spectral densities for resonant-level width $\Gamma = 0.01D$ and two impurity energies: (a) $\varepsilon_d = 0$ and (b) $\varepsilon_d = 0.05D$. The solid lines represent Eq. (60), the exact result of the procedure in Sec. III. The solid circles were obtained from Eq. (63), defined by the procedure in Ref. 5, with $\Lambda = 3$; for fixed Λ, this approach yields spectral densities at discrete energies. The triangles represent Eq. (65), the Gaussian convolution in Ref. 19, for $\Lambda = 3$. As explained in the text, the latter two approaches are reliable only near fixed points of the renormalization-group transformation $\mathcal{R}$, near the frozen-impurity fixed point ($|\varepsilon| \ll \Gamma$) in particular. Thus in (a) the solid circles and triangles describe well the resonance in the spectral density at $\varepsilon \approx \varepsilon_d$. By contrast, in (b) Eqs. (63) and (65) give spectral densities well below the maximum of the resonance.

solid lines representing the exact Eq. (60). In Fig. 2(a), this limit coincides with the center of the resonance, which is therefore well described by Eq. (63). By contrast, in Fig. 2(b), the maximum of the resonance lies in the crossover region so that for $\varepsilon \approx \varepsilon_d$ the solid circles miss the solid line by a factor of 3—the ratio between $|E_{j\pm}|\ln\Lambda$ [which divides the right-hand side of Eq. (63)] and $|dE_{j\pm}dz|$ [which divides the right-hand side of Eq. (56)]. In this case, as pointed out previously, only the procedure in Sec. III produces accurate results.

An alternative method has been more recently proposed[18,19] to smooth the discrete spectral density resulting from Eq. (53); like the procedure in Ref. 5, this approach is accurate near the frozen-impurity fixed point. To show this, Fig. 2 displays as triangles the spectral densities obtained by convoluting Eq. (53) for $z=1$ with a Gaussian:

$$\rho_d(\varepsilon)=\int_{-\infty}^{\infty}\frac{1}{\sqrt{\pi}\eta}\exp\left\{-\left[\frac{1}{\eta}\ln\left[\frac{\varepsilon_j}{\varepsilon}\right]\right]^2\right\} \times\sum_j u_{j\pm}^2\delta(\varepsilon-E_{j\pm})d\ln\varepsilon\ . \tag{65}$$

Here, as described in Ref. 19, we have carried out the integration on a logarithmic scale and taken the parameter $\eta=0.8\ln\Lambda$. For $|\varepsilon|<\Gamma$, in both cases Eq. (65) is in good agreement with Eq. (60). In particular, in Fig. 2(a) this region contains the resonance maximum. In Fig. 2(b), however, Eq. (65) reproduces poorly the maximum in the crossover region. As one might expect, therefore, the Gaussian convolution and the convolution in Ref. 5 are comparably accurate in the fixed-point region, but describe only qualitatively the crossover region.

V. LONGITUDINAL RELAXATION RATE

This section considers a spin-dependent excitation property of the $U=0$ Anderson model, the longitudinal (T_1^{-1}) relaxation rate for a spin-$\frac{1}{2}$ nucleus coupled to the impurity by the contact interaction

$$H_{i\text{-}s}=w(I_-c_{d\uparrow}^\dagger c_{d\downarrow}+I_+c_{d\downarrow}^\dagger c_{d\uparrow})\ , \tag{66}$$

where w is a constant, and I_+ (I_-) is the raising (lowering) nuclear-spin operator.

We wish to compute the temperature-dependent rate

$$\frac{1}{T_1}=\frac{2\pi}{Z(\beta)}\sum_{F,J}\exp(-\beta E_J)|\langle F|H_{i\text{-}s}|J\rangle|^2\delta(E_F-E_J)\ , \tag{67}$$

where $\beta=1/k_BT$, Z is the partition function, and $|J\rangle$, like $|F\rangle$, is an eigenstate of the unperturbed Hamiltonian H_N [Eq. (39)].

To this end, we refer to the results in Sec. III but observe that the discretization in Fig. 1 is applied to the $c_{k\uparrow}$ and $c_{k\downarrow}$ separately, two independent parameters $z_\uparrow$ and $z_\downarrow$ being introduced in this spin-degenerate case. For fixed $z_\uparrow$ and $z_\downarrow$, we then compute

$$\frac{1}{T_1}(z_\uparrow,z_\downarrow)=\frac{2\pi}{Z(\beta)}\sum_{F,J}\exp(-\beta E_J)|\langle F|H_1|J\rangle|^2\delta(E_F-E_J)\ . \tag{68}$$

The eigenstates of H_N split into a spin-up component and a spin-down component, e.g., $|F\rangle=|F\rangle_\uparrow|F\rangle_\downarrow$ and $E_F=E_{F\uparrow}+E_{F\downarrow}$. Equation (68) can therefore be written

$$\frac{1}{T_1}(z_\uparrow,z_\downarrow)=\frac{4\pi w^2}{Z_\uparrow(\beta)Z_\downarrow(\beta)}\int_{-\infty}^{\infty}\left[\sum_{F_\uparrow,J_\uparrow}\exp(-\beta E_{J_\uparrow})|\langle F_\uparrow|c_{d\uparrow}^\dagger|J_\uparrow\rangle|^2\delta(E_{F_\uparrow}-E_{J_\uparrow}-\varepsilon)\right] \times\left[\sum_{F_\downarrow,J_\downarrow}\exp(-\beta E_{J_\downarrow})|\langle F_\downarrow|c_{d\downarrow}|J_\downarrow\rangle|^2\delta(E_{F_\downarrow}-E_{J_\downarrow}+\varepsilon)\right]d\varepsilon\ , \tag{69}$$

where a factor of 2 has appeared, accounting for the (identical) contributions from the two terms on the right-hand side of Eq. (66), and an integration over ε has been introduced, to decouple the up-spin energies from the down-spin ones. Following the procedure in Sec. IV A [Eqs. (49)–(53)], we next convert the sums over the many-body states $|J\rangle$ and $|F\rangle$ into a sum over single-particle states j:

$$\frac{1}{T_1}(z_\uparrow,z_\downarrow)=4\pi w^2\int_{-\infty}^{\infty}\left[\frac{1}{1+e^{-\beta\varepsilon}}\sum_j u_{j\pm}^2\delta(E_{j\pm}-\varepsilon)\frac{e^{-\beta\varepsilon}}{1+e^{-\beta\varepsilon}}\sum_j u_{j\mp}^2\delta(E_{j\mp}-\varepsilon)\right]d\varepsilon\ , \tag{70}$$

where the upper (lower) signs refer to $\varepsilon>0$ $(\varepsilon<0)$.

Again following the procedure is Sec. IV A we now integrate this z-dependent relaxation rate, this time over $z_\uparrow$ and $z_\downarrow$, and find that

$$\frac{1}{T_1}=4\pi w^2\int_{-\infty}^{\infty}\left[[1-f(\varepsilon)]\sum_j\frac{u_{j\pm}^2}{|dE_{j\pm}/dz_\uparrow|}\bigg|_{E_{j\pm}=\varepsilon}f(\varepsilon)\sum_j\frac{u_{j\mp}^2}{|dE_{j\mp}/dz_\downarrow|}\bigg|_{E_{j\mp}=\varepsilon}\right]d\varepsilon\ , \tag{71}$$

where $f(\varepsilon)=[1+\exp(\beta\varepsilon)]^{-1}$ is the Fermi function.

Comparison with Eq. (55) now shows that each sum on the right-hand side is the impurity spectral density $\rho_d(\varepsilon)$, so that

$$\frac{1}{T_1}=4\pi w^2\int_{-\infty}^{\infty}\rho_d^2(\varepsilon)[1-f(\varepsilon)]f(\varepsilon)d\varepsilon\ . \tag{72}$$

The renormalization-group approach based on the generalized discretization in Fig. 1 therefore reproduces the exact expression,[20] applied to which standard mathematical manipulations yield the longitudinal relaxation rate.[16]

VI. CONCLUSIONS

We have generalized the renormalization-group approach,[2] a method developed to calculate thermodynamical properties of impurities in metallic environments; the extended method is capable of calculating excitation properties as well. More general than the convolution discussed in previous papers,[5] the new procedure applies to fixed-point and crossover Hamiltonians alike. As the two illustrative applications in Secs. IV and V indicate, it calculates essentially exactly the dynamical properties as functions of energy or temperature.

To make our illustrations clear, we have calculated excitation properties for a quadratic form, the resonant-level Hamiltonian. This has allowed us to compute the impurity spectral density and the longitudinal relaxation rate analytically. Applications to many-body Hamiltonians, such as that of the ($U\neq 0$) Anderson model, can only be worked out numerically. The numerical diagonalization of the truncated Hamiltonian, Eq. (23), follows the iterative procedure in Refs. 2 and 9. Although not exact, this iterative diagonalization relies on a controlled approximation;[2,9] the resulting deviations in the calculated physical properties can be made smaller than a few percent at any given temperature or frequency. An example based on the generalized method we have described, a numerical calculation of the impurity spectral density for the spin-degenerate Anderson model, has been reported in a preliminary publication.[21]

In conclusion, the discretization in Fig. 1 opens perspectives for the renormalization-group calculation of excitation properties for impurity models. The new approach may also broaden the method in a different way. In practice, the number M of states that must be kept to diagonalize iteratively each model Hamiltonian limits the number of models to which the renormalization-group approach can be applied. For increasing Λ, M decreases rapidly; the scope of the method would therefore be extended if calculations could be carried out with large Λ. Unfortunately, the computation of thermodynamical averages on the basis of the original ($z=1$) discretization produce errors proportional to $\exp(-\pi^2/\ln\Lambda)$ (with large prefactors), which become serious for $\Lambda>3$.

The generalized discretization suggests an alternative approach. Our results for the thermodynamical average evaluated in Sec. V suggest that, if a given impurity Hamiltonian is discretized and truncated as Sec. III prescribes, then diagonalized, if thermodynamical averages (such as the impurity contribution to the magnetic susceptibility or to the specific heat) are subsequently computed and these averages integrated over z, then the results, such as the right-hand side of Eq. (72), should be independent of Λ. This possibility, which would pave the road for calculations with large discretization parameters, is currently being investigated, to be discussed elsewhere.

ACKNOWLEDGMENTS

This work has been partially funded by the Brazilian Financing Agency for Studies and Projects (FINEP) and the Council for Scientific and Technological Development (CNPq). Two of us (M.Y. and M.A.W.) acknowledge support from the Foundation in Support of Research in the State of São Paulo (FAPESP). M.A.W. has been additionally supported by the Coordination for the Improvement of Higher Education (CAPES).

APPENDIX: CALCULATION OF CODIAGONAL COEFFICIENTS

This appendix develops the numerical procedure converting the conduction Hamiltonian H_c to the tridiagonal form in Eq. (13), which for convenience we write

$$H_c=H_N+\varepsilon_N^z(f_N^\dagger f_{N+1}+\text{H.c.})+R_N\ , \tag{A1}$$

where

$$H_N=\sum_{n=0}^{N-1}\varepsilon_n^z(f_n^\dagger f_{n+1}+\text{H.c.})\ , \tag{A2}$$

and

$$R_N=\sum_{n=N+1}^{\infty}\varepsilon_n^z(f_n^\dagger f_{n+1}+\text{H.c.})\ , \tag{A3}$$

so that, for $i>N$, f_i commutes with H_N, while for $i\leq N$, f_i commutes with R_N.

We want to determine the coefficients ε_n^z in Eqs. (A1) and (A2). As a preliminary step, for given integer N and non-negative integer power $n<N$, we will demonstrate the following identity:

$$f_N(H_N)^n f_0^\dagger|0\rangle\equiv 0\quad(0\leq n<N)\ , \tag{A4}$$

where $|0\rangle$ denotes the state annihilated by all c_k.

The proof is recursive. For $N=1$, Eq. (A4) becomes

$$f_1 f_0^\dagger|0\rangle=0\ , \tag{A5}$$

a self-evident equality, since the operators f_1 and f_0 are orthogonal.

Next, to complete the argument, we assume that

$$f_{N-1}(H_{N-1})^m f_0^\dagger|0\rangle=0\quad(0\leq m<N-1)\ , \tag{A6}$$

and proceed to prove Eq. (A4); to this end, for $n<N$, we consider the identity

$$(H_N)^n f_0^\dagger|0\rangle=(A+B+C)^n f_0^\dagger|0\rangle\ , \tag{A7}$$

where $A=H_{N-1}$, $B=\varepsilon_{N-1}^z f_N^\dagger f_{N-1}$, and $C=B^\dagger$.

The binomial expansion of the parentheses on the right-hand side of Eq. (A7) produces numerous terms, but

for any integer $0 \le m \le n-1$ (which implies $m < N-1$), Eq. (A6) makes $BA^m f_0^\dagger|0\rangle = 0$, while the equality $[H_{N-1}, f_N] = 0$ makes $CA^m f_0^\dagger|0\rangle = 0$. A single term ($A^n$) contributes, then, to the expansion, and Eq. (A7) becomes

$$(H_N)^n f_0^\dagger|0\rangle = (H_{N-1})^n f_0^\dagger|0\rangle \quad (0 \le n < N) . \tag{A8}$$

Since the operator f_N commutes with $(H_{N-1})^n$, Eq. (A4) follows.

This auxiliary relation established, we turn to providing another identity; to this end, we consider the state resulting from the repeated application of the Hamiltonian H_c on $f_0^\dagger|0\rangle$. According to Eq. (A1), this can be written

$$(H_c)^{N+1} f_0^\dagger|0\rangle = (\tilde{A} + \tilde{B} + \tilde{C})^{N+1} f_0^\dagger|0\rangle , \tag{A9}$$

where $\tilde{A} = H_N$, $\tilde{B} = \varepsilon_N^z f_{N+1}^\dagger f_N$, and $\tilde{C} = \tilde{B}^\dagger + R_N$.

Again, most terms in the binomial expansion of the parentheses on the right-hand side vanish. This is because (i) for $0 \le m < N$, according to Eq. (A4), $\tilde{B}\tilde{A}^m f_0^\dagger|0\rangle = 0$, and (ii) both f_{N+1} and R_N commute with $H_N \equiv \tilde{A}$, so that for any $m \ge 0$, $\tilde{C}\tilde{A}^m f_0^\dagger|0\rangle = 0$. Thus, only two terms ($\tilde{A}^{N+1}$ and $\tilde{B}\tilde{A}^N$) contribute to the expansion, and Eq. (A9) reads

$$(H_c)^{N+1} f_0^\dagger|0\rangle = (H_N)^{N+1} f_0^\dagger|0\rangle + \varepsilon_N^z f_{N+1}^\dagger f_N (H_N)^N f_0^\dagger|0\rangle . \tag{A10}$$

This equality is central to the procedure determining ε_N^z. Before discussing that procedure, however, to refine the unwieldy last term on the right-hand side of Eq. (A10) we consider the identity (A7) for $n = N$:

$$(H_N)^N f_0^\dagger|0\rangle = (A + B + C)^N f_0^\dagger|0\rangle . \tag{A11}$$

Following the reasoning that converted Eq. (A9) into Eq. (A10) we convert Eq. (A11) into

$$(H_N)^N f_0^\dagger|0\rangle = (H_{N-1})^N f_0^\dagger|0\rangle + \varepsilon_{N-1}^z f_N^\dagger f_{N-1} (H_{N-1})^{N-1} f_0^\dagger|0\rangle . \tag{A12}$$

Since f_N commutes with H_{N-1}, f_N annihilates the first term on the right-hand side. By operating with it on both sides of Eq. (A12), we then find

$$f_N (H_N)^N f_0^\dagger|0\rangle = \varepsilon_{N-1}^z f_{N-1} (H_{N-1})^{N-1} f_0^\dagger|0\rangle . \tag{A13}$$

By letting $N \to N-j$ ($j = 1, \ldots, N-1$) on both sides of this equality, we generate $N-1$ equations which, combined with Eq. (A13), yield

$$f_N (H_N)^N f_0^\dagger|0\rangle = \varepsilon_{N-1}^z \varepsilon_{N-2}^z \cdots \varepsilon_1^z f_1 \varepsilon_0^z f_1^\dagger f_0 f_0^\dagger|0\rangle , \tag{A14}$$

equivalent to

$$f_N (H_N)^N f_0^\dagger|0\rangle = \prod_{n=0}^{N-1} \varepsilon_n^z |0\rangle . \tag{A15}$$

We now substitute this expression for $f_N (H_N)^N f_0^\dagger|0\rangle$ in the last term on the right-hand side of Eq. (A10) and obtain

$$(H_c)^{N+1} f_0^\dagger|0\rangle = (H_N)^{N+1} f_0^\dagger|0\rangle + \prod_{n=0}^{N} \varepsilon_n^z f_{N+1}^\dagger |0\rangle . \tag{A16}$$

Next, we calculate the norm of both sides, obtaining

$$\langle 0| f_0 (H_c)^{2N+2} f_0^\dagger|0\rangle = \langle 0| f_0 (H_N)^{2N+2} f_0^\dagger|0\rangle + \prod_{n=0}^{N} (\varepsilon_n^z)^2 . \tag{A17}$$

In order to prove this equality identical to Eq. (14), we must now find an analytical expression for the expectation value on the left-hand side of Eq. (A17), i.e., for the norm of the state $|\Phi_{N+1}\rangle \equiv (H_c)^{N+1} f_0^\dagger|0\rangle$. Given the identity $H_c|0\rangle = 0$—which follows from the definition of $|0\rangle$—by successively commuting H_c with f_0 we find that

$$|\Phi_{N+1}\rangle = [H_c, [H_c, \cdots, [H_c, f_0^\dagger] \cdots]]|0\rangle . \tag{A18}$$

This expression, whose right-hand side nests $N+1$ commutators, effectively determines $|\Phi_{N+1}\rangle$ because an expression for the multiple commutator is easily found:

$$[H_c, [H_c, \cdots, [H_c, f_0^\dagger] \cdots]] = \left[\frac{1-\Lambda^{-z}}{2}\right]^{1/2} [a^\dagger - (-1)^N b^\dagger] [E_0(z,\Lambda)]^{N+1} + \left[\frac{1-\Lambda^{-1}}{2}\right]^{1/2} \sum_{m=1}^{\infty} \Lambda^{(1-z-m)/2} [E_m(z,\Lambda)]^{N+1} [a_m^\dagger - (-1)^N b_m^\dagger] . \tag{A19}$$

The norm $\langle \Phi_{N+1} | \Phi_{N+1} \rangle \equiv F_N(z,\Lambda)$ is therefore

$$F_N(z,\Lambda) = (1-\Lambda^{-1}) \sum_{m=1}^{\infty} \Lambda^{1-z-m} [E_m(z,\Lambda)]^{2N+2} + (1-\Lambda^{-z}) [E_0(z,\Lambda)]^{2N+2} . \tag{A20}$$

This expression for $F_N(z,\Lambda)$ is finally substituted for the left-hand side of Eq. (A17), which then yields Eq. (14).

[1] N. Andrei, K. Furuya, and J. H. Lowenstein, Rev. Mod. Phys. **55**, 331 (1983); A. M. Tsvelick and P. B. Wiegmann, Adv. Phys. **32**, 453 (1983).

[2] K. G. Wilson, Rev. Mod. Phys. **47**, 773 (1975).

[3] J. Hirsch and R. Fye, Phys. Rev. Lett. **55**, 1355 (1985).

[4] N. E. Bickers, Rev. Mod. Phys. **59**, 845 (1987).

[5] L. N. Oliveira and J. W. Wilkins, Phys. Rev. B **24**, 4863 (1981); D. L. Cox, H. O. Frota, L. N. Oliveira, and J. W. Wilkins,

ibid. **32**, 555 (1985); L. N. Oliveira and J. W. Wilkins, *ibid.* **32**, 696 (1985); D. L. Cox, Ph.D. thesis, Cornell University, Ithaca, New York, 1985.

[6]P. W. Anderson, Phys. Rev. **124**, 41 (1961).

[7]See, e.g., J. N. Miller, D. T. Ling, P. M. Stefan, D. L. Weissman, M. L. Shek, I. Lindau, and W. E. Spicer, Phys. Rev. B **24**, 1917 (1981).

[8]S. L. Rudaz, J. P. Ansermet, P. K. Wang, C. P. Slichter, and J. Sinfelt, Phys. Rev. Lett. **54**, 71 (1985); J. P. Ansermet, P. K. Wang, C. P. Slichter, and J. Sinfelt, Phys. Rev. B **37**, 1417 (1988).

[9]H. R. Krishna-murthy, J. W. Wilkins, and K. G. Wilson, Phys. Rev. B **21**, 1003 (1980).

[10]H. R. Krishna-murthy, J. W. Wilkins, and K. G. Wilson, Phys. Rev. B **21**, 1044 (1980).

[11]P. Nozières and C. T. De Dominicis, Phys. Rev. **178**, 1097 (1969).

[12]M. Yoshida and L. N. Oliveira (unpublished).

[13]Equation (9) applies to dispersion relations that are odd in the momenta measured from the Fermi level. For other dispersion relations, the positive and the negative discrete energies would be asymmetric.

[14]For a review, see R. Haydock, in *Solid State Physics,* edited by H. Ehrenreich, F. Seitz, and D. Turnbull (Academic, New York, 1980), Vol. 35, p. 215.

[15]That the ε_N^z can be easily obtained numerically from Eqs. (14) and (16) is an important convenience of our approach, since the algebra involved in solving those equations becomes very tedious for $N > 3$.

[16]M. Salomaa, Z. Phys. B **25**, 49 (1976).

[17]As indicated in Ref. 5, the discretization for the conduction band renormalizes the model parameters. In particular, in the resonant-level model the coupling V is reduced to the effective value $V/\sqrt{A_\Lambda}$, where A_Λ is defined by Eq. (46), while ε_d is not changed. To compensate for the renormalization, the parameter V entering the actual calculations is multiplied by $\sqrt{A_\Lambda}$.

[18]D. E. Heim, Phys. Rev. B **33**, 5254 (1986).

[19]O. Sakai, Y. Shimizu, and T. Kasuya, J. Phys. Soc. Jpn. **58**, 3666 (1989).

[20]C. P. Slichter, *Principles of Magnetic Resonance* (Springer-Verlag, Berlin, 1978).

[21]H. O. Frota and L. N. Oliveira, Phys. Rev. B **33**, 7871 (1986).